Electrical component ignition in a closed enclosure adjacent to a controlled fire

Pascal Zavaleta, Olivier Bouygues, Céline Lapuerta

HAL Id: irsn-04066759
https://irsn.hal.science/irsn-04066759

Submitted on 12 Apr 2023

IGNITION OF ELECTRICAL COMPONENTS CONTAINED IN A CLOSED ENCLOSURE ADJACENT TO A CONTROLLED FIRE SOURCE

Pascal Zavaleta, Olivier Bouygues and Céline Lapuerta

Institut de Radioprotection et de Sûreté Nucléaire (IRSN), PSN-RES, SA2I, Cadarache, St Paul-Lez-Durance Cedex, 13115, France

ABSTRACT

Electrical cabinet fires are one of the main fire hazards in nuclear power plants (NPPs). The electrical cabinets are often arranged in rows of adjacent cabinets in NPPs. So the ability of a cabinet fire to spread to adjacent cabinets is a major concern for fire safety. This work aims at investigating the impact on the fire spread of the air gap between two electrical cabinets, the electrical component-type contained in the adjacent cabinet and its ventilation mode. For that purpose, a test device composed of two adjacent steel enclosures was designed in order to reproduce at reduced-scale adjacent electrical cabinets. This study first reveals that the studied electrical component-types spontaneously ignited when their temperature and the incident heat flux reach critical ignition values. These ignition criteria are assessed for each component-type. The tests also show that the air gap increase slows down the rise of the side wall temperature of the two enclosures, which delays the ignition time of the electrical components. This work finally highlights that the mechanical ventilation of the adjacent enclosure has an impact on the ignition conditions. In contrast, the natural ventilation as implemented in the adjacent enclosure has a small effect on these conditions.

NOMENCLATURE

AE	Adjacent enclosure
ATH	Alumina trihydrate
AW	Adjacent wall
EVA	Ethylene-vinyl acetate
FE	Fire enclosure
FW	Fire wall
g	Air gap between the adjacent enclosures
HFFR	Halogen-free flame retardant
IHF	Incident heat flux (kW/m^2)
$\dot{q}^{"}$	Incident heat flux measured close to the target (kW/m^2)
$\dot{q}^{"}_{ig}$	Incident heat flux measured close to the target at its ignition time (kW/m^2)
$\dot{q}^{"}_{c,ig}$	Critical ignition heat flux (kW/m^2)
PE	Polyethylene
PVC	Poly(vinyl chloride)
$\tilde{u}$	Relative uncertainty of a measurement (-)
$\tilde{U}$	Expended relative uncertainty of a measurement (-)
$\tilde{u}_i$	Relative instrument uncertainty (-)
$\tilde{u}_r$	Relative uncertainty component for repeatability (-)
TB	Terminal block
$T_{av,AE}$	Average gas temperature in the AE (°C)
$T_{av,Z}$	Average temperature of the outer AW (Z = AW) or FW (Z = FW) (°C)
$T^{ig}_{av,Z}$	Average temperature of the outer AW (Z = AW) or FW (Z = FW) at the target ignition (°C)

$T_{av,Z}^{ig,k}$	Average temperature of the outer AW (Z = AW) or FW (Z = FW) at the target ignition for the test k (°C)
$T_{Z\_X\_Y}$	Temperature measurement of the outer FW (Z = FW) or the AW (Z = AW) at the coordinates X = 100 or 500 mm and Y = 100, 500 or 900 mm
$T_{c,ig}$	Critical ignition temperature (°C)
t_{ig}	Ignition time (s)
XLPE	Cross-linked polyethylene

INTRODUCTION

Nearly four hundred fire events in Nuclear Power Plants (NPPs) were recorded since the 1980's to the end of 2010 in the current OECD FIRE Database[1]. Almost fifty fire events involved electrical cabinets[2] which are commonly arranged in rows of adjacent cabinets. It is also argued[2] that a cabinet fire in a control or switchgear room of NPPs could lead to failure of one safety train or more, if fire spreads beyond the fire cabinet. So the ability of a cabinet fire to spread to adjacent cabinets is a major concern for fire safety in NPPs.

Few studies investigated the fire spread from one cabinet to adjacent ones. Mangs *et al.*[3] conducted nine full-scale fire experiments which involved two types of vertical closed-doors electronic cabinets. The electronic cabinets were mainly equipped either with relays or circuit boards and they also all contained electric cables with poly(vinyl chloride) (PVC) jackets. The electronic cabinets, called the fire cabinets, were ignited in all experiments with a propane gas burner. A mock-up cabinet made of thin steel sheets (0.5 mm thick) was attached to the fire cabinet (ie, there was no gap between the cabinets) to study the response of an adjoining cabinet to the fire. For four fire experiments, the adjacent cabinet contained samples of five PVC cables 400 mm long attached to the wall against the fire cabinet, and also placed at 5 and 30 cm from this wall. For two of these experiments, which led to a flashover in the fire cabinet, the PVC cables contained inside the adjacent cabinet ignited. So the spread of fire to an adjacent and fastened cabinet is possible because of heating of the separating walls.

Furthermore, Zavaleta *et al.*[4] studied the fire spread from an open-door twin modules 400 V electro-technical cabinet to two adjacent closed-door cabinets. The central open-door cabinet, which can be found in French nuclear installations, was fully and previously characterised by Coutin[5] and Coutin *et al.*[6]. The main components inside the central cabinet were transformers, terminal blocks, motor circuit breakers and contactors, relays, circuit breakers, vertical trunkings, horizontal trunkings and electric cables. A propane burner located at the bottom of the central cabinet was used to ignite it. This burner provided a fire power of about 10 kW for a duration of about 5 minutes. For one fire test, two closed-door electrical cabinets were placed against the side walls of the central open-door cabinet without no gap between the cabinets. These adjacent cabinets were cabinet modules identical to the twin modules of the central cabinet and their side walls were 1.5 mm thick. Each adjacent cabinet was equipped with targets composed of PVC trunkings placed against the adjacent side wall and that contained either PVC or halogen free flame retardant (HFFR) cable samples. This fire test showed that the targets composed of PVC trunkings filled with the PVC electric cables burnt while the ignition of the HFFR electric cables was not highlighted. So the spread of fire to a fastened cabinet may depend on the target type contained inside.

Therefore, for completing the previous studies, investigations were carried out for providing new insights on the ignition of electrical components that can potentially occur in an electrical cabinet adjacent to another burning cabinet. This work especially aims at studying the impact on the ignition conditions of the electrical component-type (bundles of electric cables or sets of terminal blocks) contained in the adjacent electrical cabinet and the air gap between the cabinets (in the 1-5 cm range). This study also discusses ignition criteria which are assessed for each electrical component-type. Furthermore, the effects of the ventilation mode of the adjacent cabinet on the ignition conditions are also addressed in this work. Electrical cabinets in nuclear facilities[7,8] may be indeed either not ventilated or ventilated (naturally or mechanically).

For that purpose, a reduced-scale test device of adjacent electrical cabinets[4] was designed. This test device is composed of two adjacent steel enclosures separated by an air gap. The first enclosure, that contains a gas burner at its bottom, corresponds to a one-quarter scale model of the open-door

electrical cabinet studied in previous works[4-6]. The second enclosure, that contains electrical components, considered as targets in this study, reproduces at reduced scale the adjacent cabinets[4].

The first part of this work presents the experimental matrix, the reduced-scale experimental set-up, the related instrumentation and the test protocol. The second part of this study first deals with the test repeatability and also aims at assessing the measurement uncertainties. Next, this part, based on a result analysis, discusses the ignition mechanisms and proposes ignition criteria which are assessed for the studied target-types. This part finally presents the effects on the ignition conditions of the air gap and the ventilation mode as implemented in the adjacent enclosure.

FIRE TEST DESCRIPTION

Eleven fire tests were carried out to study the impact on the ignition conditions of the air gap between the two adjacent enclosures (in the 1-5 cm range), the target-type (sets of terminal blocks [TB] or bundles composed of either PVC or HFFR electric cables) and the adjacent enclosure ventilation mode (without ventilation, natural or mechanical), as summarized in Table 1. Furthermore, the setups of T3 and T7 tests are identical to those of the T2 and T6 tests, respectively. The outcomes of these tests will be further used to evaluate the test repeatability.

Table 1 : Fire test matrix

Test ID	Target type	Air gap (cm)	Ventilation mode
T1	Bundle of PVC cables	1	Without
T2	Bundle of PVC cables	3	Without
T3*	Bundle of PVC cables	3	Without
T4	Bundle of PVC cables	3	Natural
T5	Bundle of PVC cables	1	Mechanical
T6	Bundle of HFFR cables	1	Without
T7*	Bundle of HFFR cables	1	Without
T8	Sets of TB	1	Without
T9	Sets of TB	3	Without
T10	Sets of TB	3	Natural
T11	Sets of TB	5	Without

* Repeatability test. Abbreviations: HFFR, halogen-free flame retardant; PVC, poly(vinyl chloride); TB, terminal block.

Experimental setup

The test device (Fig. 1) is composed of two adjacent steel enclosures 0.6 m wide, 0.6 m deep, 1 m high and separated by an air gap (Fig. 2). The design of this test device was based on a scale reduction of adjacent electrical cabinets studied by Zavaleta *et al*[4]. This cabinet set-up (Fig. 3) was composed of a twin modules 400 V electro-technical open-door cabinet, used as the fire cabinet, and two adjacent closed-door cabinets. These last ones, placed against the side walls of the central cabinet, were cabinet modules identical to the twin modules of the central open-door cabinet. The design of the reduced-scale test device followed the successive steps:

- provided the symmetry plane of the real-scale cabinet set-up (Fig. 3), only its half part was considered (ie, one module of the open-door central cabinet and one adjacent closed-door cabinet module),
- then, a height reduction of a factor two was applied for the two modules.

The left-hand enclosure (Fig. 1), named the fire enclosure (FE), therefore corresponds to one-quarter scale model of the central open-door electrical cabinet[4] (1.2 m wide, 0.6 m deep and 2 m high). An insulated panel was placed against the internal left-hand side wall of the FE to simulate the symmetry plane. Furthermore, the front panel of the FE was removed (as for the open-door electrical cabinet) and a gravel-packed gas burner 0.5 m x 0.5 m was located at its bottom. This last one provided a constant fire power of 300 kW for all the tests, which corresponds to one fourth of the maximum heat release rate of the studied open-door cabinet[4] characterized in open atmosphere[6]. This thus allows to get the same fire power per unit volume for the reduced and real-scales. Furthermore, the work[4] also showed that electrical components contained in the adjacent cabinets ignited when the side wall temperature of the fire cabinet exceeded 600°C, as illustrated in Fig. 4. Numerical simulations were performed with the CALIF3S/ISIS fire field model[9] to confirm that the above design of the FE allowed to reach side wall temperature higher than 600°C. A schematic of the computational domain of dimensions 1.2 m x 1.8 m x 1.5 m is represented in Fig. 5. A symmetry condition was applied for x = 0 and the floor is considered as an adiabatic boundary. The red surface in Fig. 5 represents the gas diffusion burner. A multi-domain approach is used to compute both the flow and the temperature in the steel walls of the fire enclosure. The total mesh number is 31700 for the fluid domain and 100000 for the solid domain which is mainly represented by the FE surfaces. The gas burner was modelled by a fuel injection boundary condition using a mass loss rate determined from the ratio between the fixed fire power and the effective heat of combustion for propane (43.7 x 10^6 J.kg^{-1}). In addition, wall-type boundary conditions were considered for the steel walls of the FE. The thickness of the steel walls of the fire enclosure was 0.003 m and the emissivity was fixed to 0.8. Fig. 6 shows the average temperature of the right side wall of the FE calculated for four power values of the gas burner (ie, 100, 200, 300 and 400 kW). The results point out that the wall temperatures calculated for the two higher fire powers are very similar and both exceeding 600°C. Numerical simulations thus confirm that the above criterion is obtained for a fire power of 300 kW.

The right-hand side enclosure is called the adjacent cabinet (AC). The adjacent walls of the FE and AE, named the fire wall (FW) and adjacent wall (AW), respectively, are shown in Fig. 2. The thicknesses of the FW and AW are 3 and 1.5 mm, respectively. The lower thickness was the same as for the side walls of the adjacent electrical cabinets[4]. A larger thickness was considered for all the walls of the FE for ensuring its resistance to thermal stresses as long as possible.
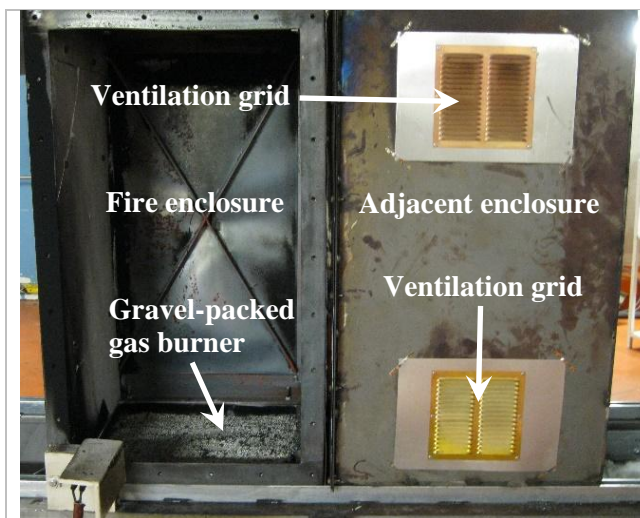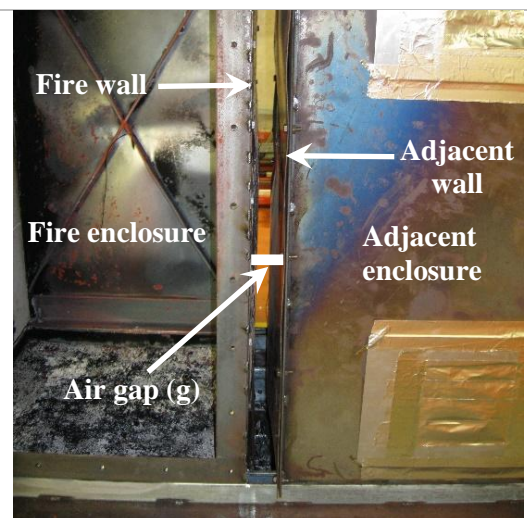

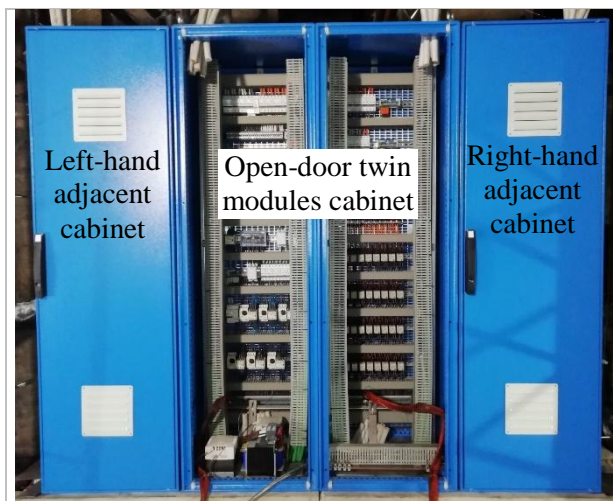| Fig. 1: Fire and adjacent enclosures. | Fig. 2: Air gap (g) between the two enclosures (eg, for the T11 test, g = 5 cm). |

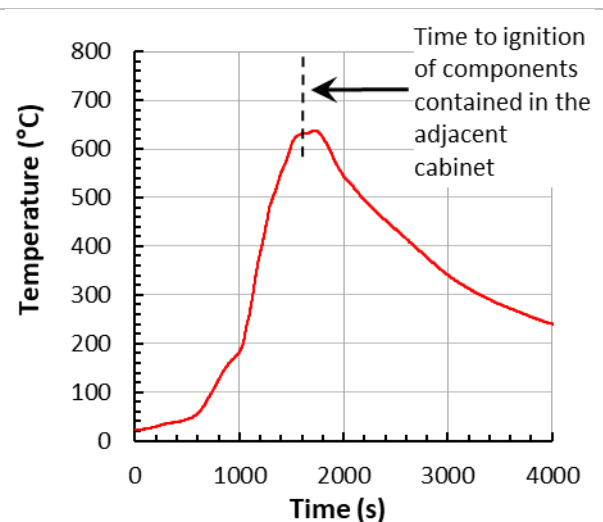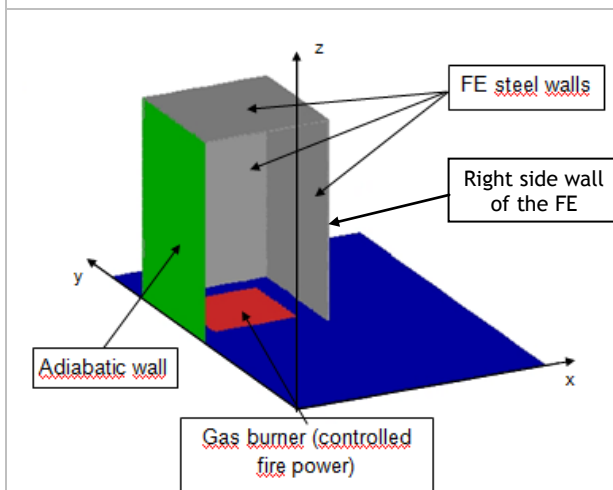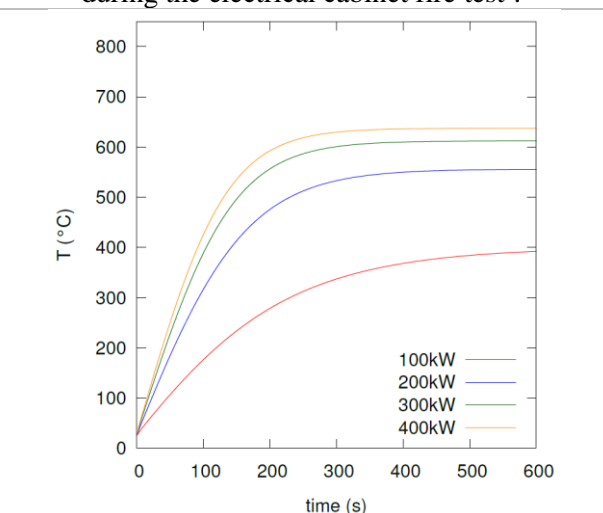|	
Fig. 3: The adjacent electrical cabinet set-up[4].	Fig. 4: Average side wall temperature measured during the electrical cabinet fire test[4].
Fig. 5: Fire enclosure modelling with the CALIF3S/ISIS software[9].	Fig. 6: Average right side wall temperature of the fire enclosure calculated with the CALIF3S/ISIS software[9].

Electrical components used as targets

Terminal blocks (TB) and samples of either PVC or HFFR cables were used to compose the three target-types considered in this study:
- three sets of forty TB each one (Fig. 7),
- a bundle of ten cable samples 1 m long of the HFFR cable-type (Fig. 8),
- a bundle of ten cable samples 1 m long of the PVC cable-type (Fig. 9).

Table 2 gives more specifications of the elements of these target-types which are electrical components commonly found close to the side walls of electrical cabinets present in nuclear power plants (NPPs)[4,7,8]. The targets were positioned close to the AW and supported by a grid fixed to the rear panel of the AE (Fig. 7 and Fig. 8). The distance of the targets from the AW was always lower than 1 cm. Therefore, the targets were either very nearly or in contact with the AW.
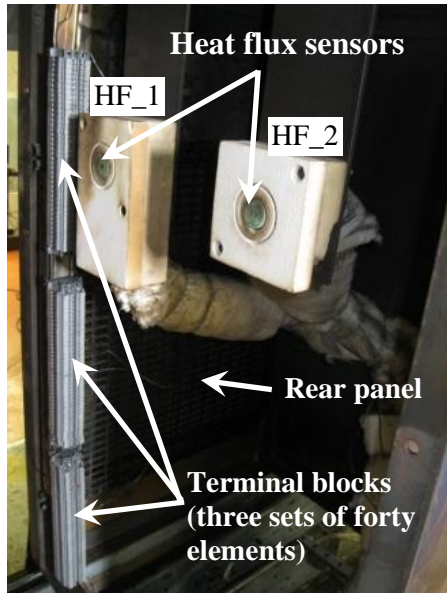
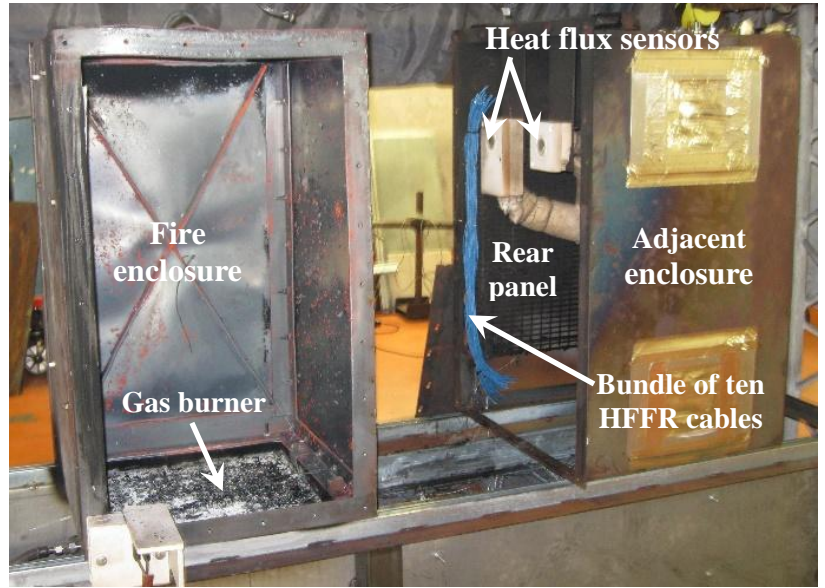Fig. 7: Inside the adjacent enclosure (AW removed).

Fig. 8: Test device before the side wall of the adjacent enclosure is installed.

Table 2 : Specifications of the electrical components composing the targets.

Electrical component	Supplier specification	Chemical composition
HFFR electric cable	VARPREN ST 1.5 mm^2 Halogen Free	EVA, PE and ATH as HFFR
PVC electric cable	U1000R02V 3x2.5 mm^2	PVC for external sheath XLPE for insulation
TB	TB 4/6 1SNA 115 116 R0700	Polyamide

Abbreviations: ATH, Alumina trihydrate; EVA, Ethylene-vinyl acetate; HFFR, halogen-free flame retardant; PE, Polyethylene; PVC, poly(vinyl chloride); TB, terminal block; XLPE, Cross-linked polyethylene.

Ventilation of the adjacent enclosure

The front panel of the AE was equipped with two ventilation grids of unit surface of 0.03 m^2 (Fig. 1).
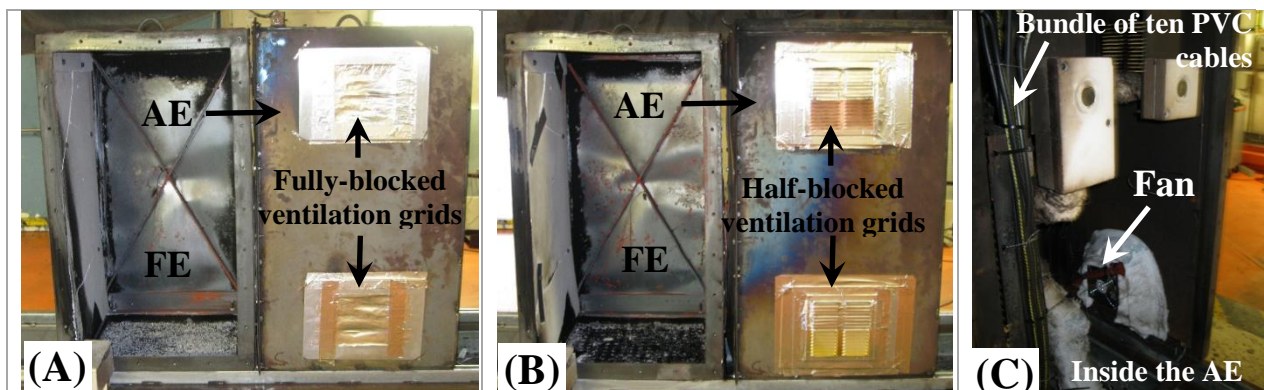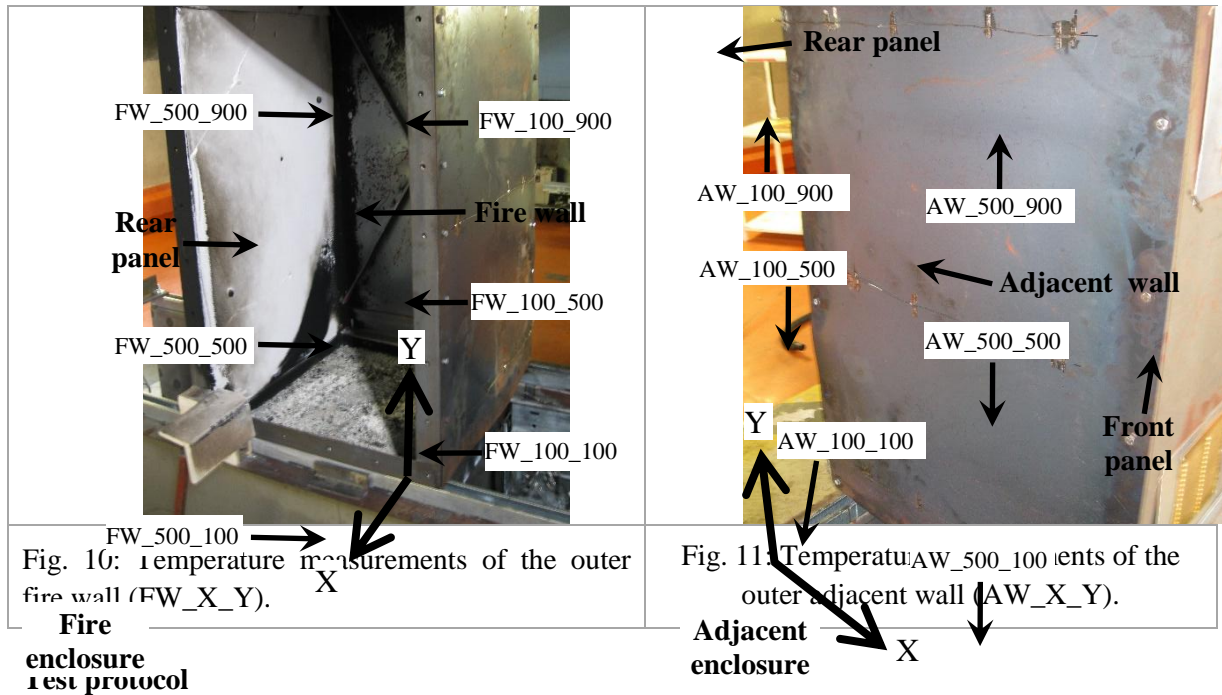

Fig. 9: Ventilation mode of the AE. A, No ventilation. B, Natural ventilation. C, Mechanical ventilation. FE, fire enclosure; AE, adjacent enclosure; PVC, poly(vinyl chloride).

The studied ventilation mode was either without ventilation (ie, the grids were fully-blocked), natural (ie, the grids were half-blocked) or mechanical (ie, a fan was connected to the bottom grid and the two grids were fully unobstructed), as illustrated in Fig. 9. In the last case, the ventilation flow rate was set at 165 m^3/h in the AE. This value is indeed about the half of the ventilation flow rate (300 m^3/h) used in the adjacent electrical cabinets[4] (0.72 m^3 in volume) used to design the AE (0.36 m^3), as earlier discussed.

Instrumentation

Temperature measurements of the outer FW and outer AW were carried out using six 0.5 mm K-type thermocouples brazed on each of these walls (Fig. 10 and Fig. 11). Temperature measurements in the AE were performed thanks to twelve 1.5 mm K-type thermocouples positioned in the four corners of this enclosure at three heights (100, 500 and 900 mm from the bottom of the AE), as indicated in Fig. 12. Finally, the incident heat fluxes (IHF) in the AE were measured using two Gardon-type heat flux sensors positioned at about 10 mm from the AW (Fig. 7 and Fig. 8). Table 3 summarizes the above measurements and also fully specifies the location of the related sensors in the test device. The relative uncertainties for the instruments, $\tilde{u}_i$, are given in Table 4[*]. These values of $\tilde{u}_i$ were deduced from calibration tests conducted for each sensor before its use for the fire tests presented in this work.

Fig. 10: Temperature measurements of the outer fire wall (FW_X_Y).

Fig. 11: Temperature measurements of the outer adjacent wall (AW_X_Y).

Test protocol

The fire tests were conducted under a large-scale calorimeter in open atmosphere conditions. The eleven fire tests, T1 to T11, were carried out with the same test protocol: the controlled fire with a power of 300 kW was maintained until few time after the ignition of the target in the AE. Fig. 13 illustrates the test protocol for example for the T1 test and Fig. 14 shows the FE and AE during the same fire test.

---

[*]The uncertainty (or standard deviation) of the instrument for a given measurement (u_i, expressed in the same unit as the related measurement) can be deduced from the product of $\tilde{u}_i$ by the value of the measurement.
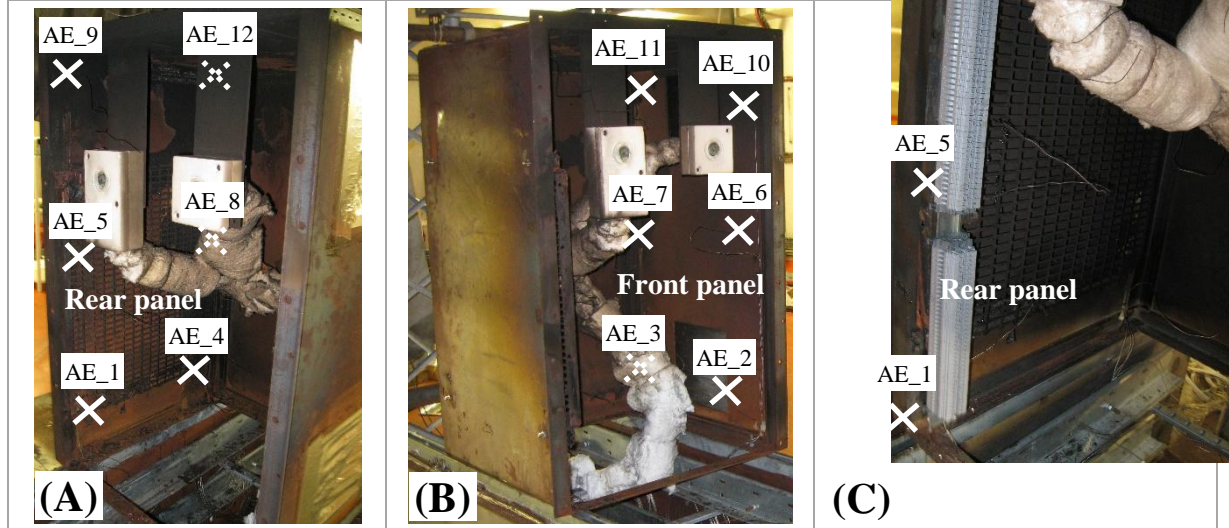
Fig. 12: Temperature measurements in the AE (AW removed). A, close to the rear panel. B, close to the front panel. C, inside the targets (eg, in the TB). The cross indicate approximately the TC location (dash-lined cross means that the TC is hidden by an equipment). TC, thermocouple.

Table 3: Measurements used in this study.

Measurement ID	Measurement	Sensor	Location
FW_X_Y	Temperature of the outer FW.	0.5 mm K-type thermocouple (TC)	X = 100 and 500 mm from the rear panel of the FE. Y = 100, 500 and 900 mm from the bottom of the FE (Fig. 10).
AW_X_Y	Temperature of the outer AW.	0.5 mm K-type TC	X = 100 and 500 mm from the rear panel of the AE. Y = 100, 500 and 900 mm from the bottom of the AE (Fig. 11).
AE_1 to AE_12	Temperature in the AE.	1.5 mm K-type TC	AE_1 to 4, AE_5 to 8, AE_9 to 12 located at 100, 500 and 900 mm from the bottom of the AE, respectively (Fig. 12). For each height, the TC were located in the four corners of the AE at about 5 cm from the panels. AE_1, 5 and 9 were placed in the targets.
HF_1 and HF_2	IHF in the AE.	Gardon-type heat flux sensor	HF_1 and HF_2 located at 175 mm from the rear and front panel, respectively, at 250 mm from the ceiling and at about 10 mm from the AW (Fig. 7).

Abbreviations: AE, adjacent enclosure; AW, adjacent wall; FE, fire enclosure; FW, fire wall; HF, heat flux; IHF, Incident heat flux.

Fig. 13 especially shows the IHF in the AE measured close to the targets[†], $\dot{q}''$ and the average temperatures of the outer FW and AW, $T_{av,FW}$ and $T_{av,AW}$, respectively. These average temperatures are calculated as follows:

[†] The heat flux measurements presented in this work were always carried out with the heat flux sensor HF_1 which was located closer to the target than the second one HF_2 (Fig. 7).

$$T_{av,Z} = \frac{1}{6} \cdot \sum_{\substack{X=100;500 \\ Y=100;500;900}} T_{Z\_X\_Y}$$

(1)

Where Z = FW or AW, $T_{Z\_X\_Y}$ are the six temperature measurements of the outer FW (Z = FW, Fig. 10) or the six ones of the outer AW (Z = AW, Fig. 11), and X = 100 or 500 mm and Y = 100, 500 or 900 mm, are the related coordinates as specified in Table 3. The targets were thus submitted to an increasing IHF emitted by the AW which is heated by the FW itself in contact with the controlled fire. Finally, it can be noticed that $T_{av,FW}$ is higher than 600°C for the T1 test (Fig. 13) as it was predicted by the 3D simulations for a fire power of 300 kW (Fig. 6). Such values for $T_{av,FW}$ were also obtained for all the tests as further shown.

Table 4 : Relative instrument uncertainty ($\tilde{u}_i$).

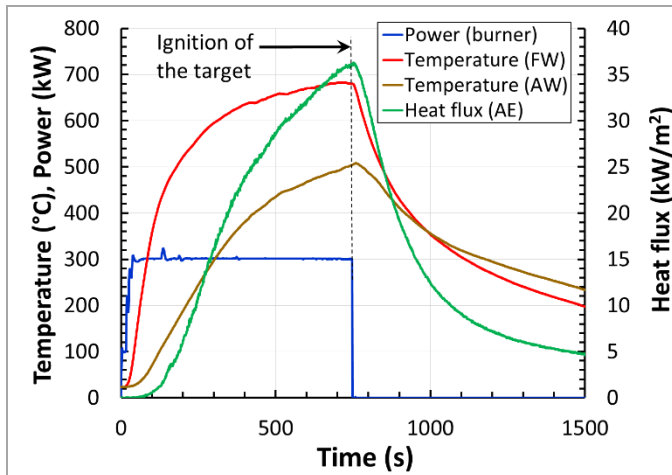| Sensor type	$\tilde{u}_i$ (-)
1.5 mm K-type thermocouple	0.025
0.5 mm K-type thermocouple	0.025
Gardon-type heat flux sensor	0.03

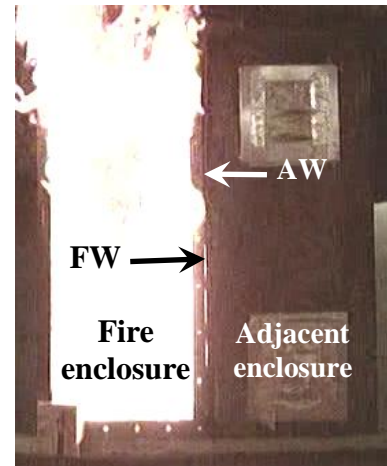|	
Fig. 13: Illustration of the test protocol (eg, for the T1 test). FW, fire wall; AW, adjacent wall; AE, adjacent enclosure.	Fig. 14: The fire and adjacent enclosures during a fire test (eg, for the T1 test). AW, adjacent wall; FW, fire wall.

RESULTS AND DISCUSSION

The following section first comments test repeatability and also describes how are assessed the uncertainties of the measurements. Next, target ignition criteria are proposed and their variation according to the target-type is discussed. Finally, the impact of the air gap and the ventilation mode of the AE on the wall temperatures, heat flux in the AE and the ignition conditions are especially commented.

Test repeatability and measurement uncertainties

The T3 and T7 tests repeated the T2 and T6 tests, respectively, as earlier commented (Table 1). Fig. 15 to Fig. 17 compare time evolutions of $T_{av,FW}$, $T_{av,AW}$ and $\dot{q}''$, respectively, for both the T2 and T3 tests. Furthermore, Fig. 18 to Fig. 20 show also the time evolutions of the three above parameters for both the T6 and T7 tests. The ignition time of the targets (t_{ig}) are also indicated in the above figures. All these figures highlight for the T2/T3 and T6/T7 tests a satisfactory test repeatability that can be assumed for all the T1 to T11 tests which followed the same test protocol.
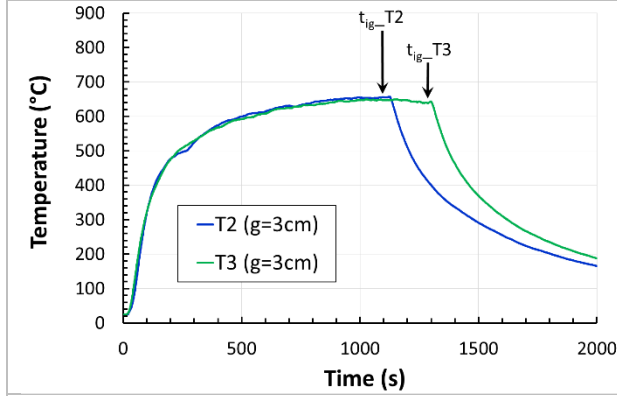

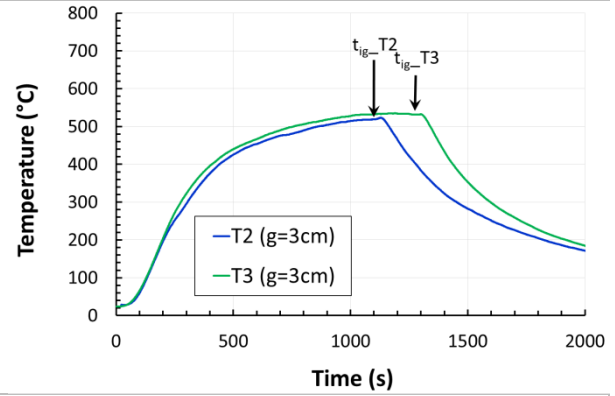Fig. 15: Average temperature of the FW for the T2 and T3 tests. FW, fire wall.

Fig. 16: Average temperature of the AW for the T2 and T3 tests. AW, adjacent wall.
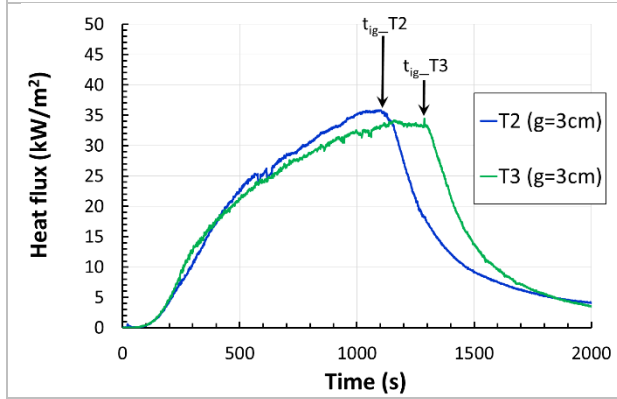

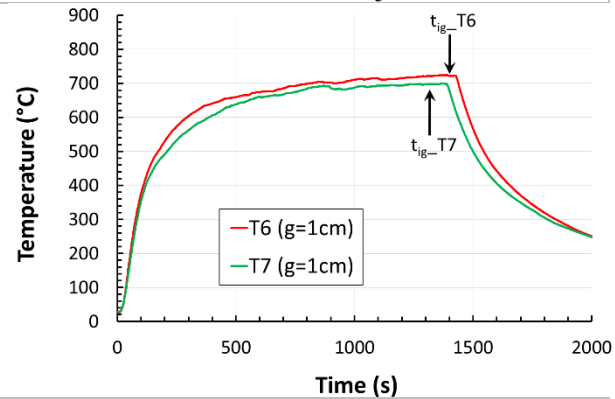Fig. 17: IHF[†] in the AE for the T2 and T3 tests. IHF, incident heat flux; AE, adjacent enclosure.

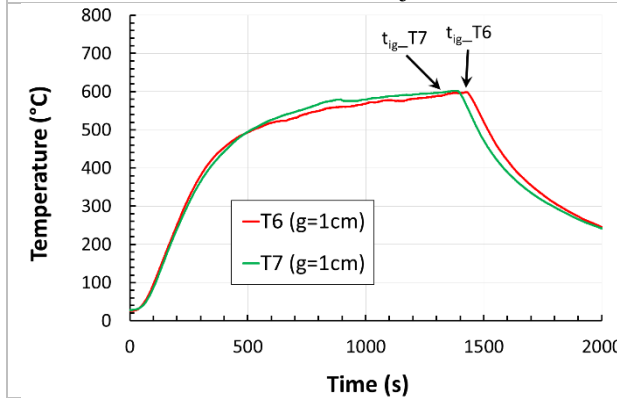Fig. 18: Average temperature of the FW for the T6 and T7 tests. FW, fire wall.

Fig. 19: Average temperature of the AW for the T6 and T7 tests. AW, adjacent wall.
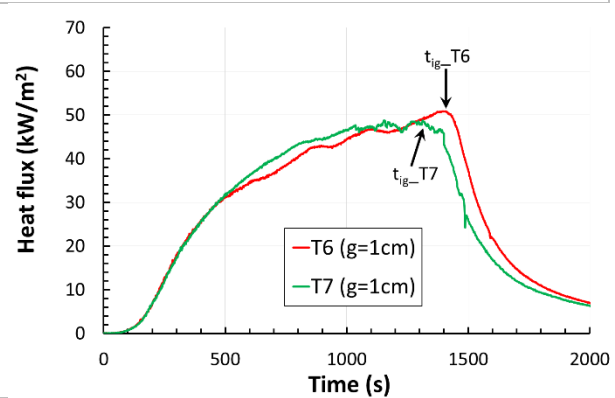

Fig. 20: IHF in the AE for the T6 and T7 tests. IHF, incident heat flux; AE, adjacent enclosure.

The relative uncertainty of a measurement, $\tilde{u}$, may be estimated by combining the individual relative uncertainties, such as the relative instrument uncertainty ($\tilde{u}_i$, Table 4) and the relative uncertainty

component for repeatability, $\tilde{u}_r$[‡], using the usual method called the "law of propagation of uncertainty"[10,11]. $\tilde{u}$ is thus evaluated as follows:

$$\tilde{u} = \sqrt{\tilde{u}_i^2 + \tilde{u}_r^2} \tag{2}$$

Furthermore, the uncertainty is often expressed in terms of an expanded uncertainty, in which the confidence level that the measurement falls within the expanded bounds is high[10]. For an expansion factor (or coverage factor) of 2, considered in this study, the expanded relative uncertainty of the measurement, $\tilde{U}$, is thus related to two relative standard deviations (i.e., $2 \cdot \tilde{u}$) and the confidence level corresponds to 95 %. Table 5 provides $\tilde{u}_r$ estimated for $T_{av,FW}$, $T_{av,AW}$ and $\dot{q}^{"}$. First, $\tilde{u}_r(T_{av,FW})$ is assessed as the maximal of the average of the relative deviation between $T_{av,FW}$ measured for the T2 ($T_{av,FW}^{T2}$) and T3 ($T_{av,FW}^{T3}$) tests and that measured for the T6 ($T_{av,FW}^{T6}$) and T7 ($T_{av,FW}^{T7}$) tests:

$$\tilde{u}_r(T_{av,FW}) = \max\left(\frac{1}{N}\sum_{i=1}^{N}\frac{|T_{av,FW}^{T2}(t_i) - T_{av,FW}^{T3}(t_i)|}{T_{av,FW}^{T2}(t_i)}; \frac{1}{K}\sum_{i=1}^{K}\frac{|T_{av,FW}^{T6}(t_i) - T_{av,FW}^{T7}(t_i)|}{T_{av,FW}^{T6}(t_i)}\right) \tag{3}$$

Where N and K are the measurement numbers[§] of $T_{av,FW}^{T2}/T_{av,FW}^{T3}$ and $T_{av,FW}^{T6}/T_{av,FW}^{T7}$, respectively, considered in Eq. (3), t_1 is the starting time of the tests, t_N and t_K correspond with the earliest ignition time of the target between the T2 and T3 tests (ie, $t_{ig\_}T2$, Fig. 15) and that between the T6 and T7 tests (ie, $t_{ig\_}T7$, Fig. 18), respectively. $\tilde{u}_r(T_{av,AW})$ and $\tilde{u}_r(\dot{q}^{"})$ are then estimated in the same way as $\tilde{u}_r(T_{av,FW})$. Finally, $\tilde{u}$ is evaluated according to Eq. (2) and the estimates of both $\tilde{u}_i$[**] (Table 4) and $\tilde{u}_r$ (Table 5). Table 5 also gives $\tilde{U}$ (ie, $2 \cdot \tilde{u}$) for $T_{av,FW}$, $T_{av,AW}$ and $\dot{q}^{"}$.

Table 5 : Relative uncertainty component for repeatability ($\tilde{u}_r$) and expanded relative uncertainty of the measurements ($\tilde{U}$).

Measurement (unit)	$\tilde{u}_r$ (-)	$\tilde{U}$ (-)
Average temperature of the outer FW, $T_{av,FW}$ (°C)	0.04	0.08
Average temperature of the outer AW, $T_{av,AW}$ (°C)	0.04	0.08
IHF measured close to the target, $\dot{q}^{"}$ (kW/m²)	0.08	0.17

Abbreviations: AW, adjacent wall; FW, fire wall; IHF, Incident heat flux.

Ignition mechanisms and criterion

Fig. 21 shows, for instance for the T2 test, the inside of the AE two hundredth of seconds before the ignition of the target (bundle of ten PVC cables). The following events, successively illustrated in Fig. 22 to Fig. 24, were then observed:

(1) First at t_{ig}, a localized ignition in the central part of the target (Fig. 22) that leads to the sudden increase of the related temperature measurement (AE_5) located nearby (Fig. 25),

---

[‡] While $\tilde{u}_i$ gives the (relative) uncertainty of an instrument in advantageous conditions during calibration tests, $\tilde{u}_r$ aims at quantifying the impact of the fire test conditions on the measurement uncertainty.

[§] One measurement recorded per second.

[**] Given that $T_{av,AW}$ and $T_{av,FW}$ are evaluated from Eq. (1), the relative instrument uncertainty of these measurements can be evaluated as follows[10]: $\tilde{u}_i(T_{av,AW}) = \tilde{u}_i(T_{av,FW}) = \frac{1}{6} \cdot \sqrt{u_i^2 \cdot 6} \sim 0.01$ where $\tilde{u}_i = 0.025$ for each temperature measurement of the outer FW and outer AW (0.5 mm K-type TC, table 4).

(2) A couple of hundredth of seconds later, the localized flame on the target ignited the accumulated flammable gases within all the AE volume (Fig. 23),

(3) Few tenths of seconds later, fire rapidly spread along the target beyond the ignition zone (Fig. 24). In most tests, fire spread over a significant part or the totality of the target.

The video analysis of all the tests highlights similar ignition mechanisms. Only the localisation of the ignition along the target can change according to the test. Furthermore, a question is arisen from the above description: is the ignition either piloted or spontaneous? Piloted ignition is generally achieved through localized heating such as an electric spark, a small flame or a heated wire, and the flame then propagates into the rest of the fuel material[12]. In contrast, spontaneous or self-ignition occurs as a result of raising the bulk temperature of a combustible gas mixture, and does not require any further external heat supply once combustion has started[13]. A spontaneous ignition requires a higher temperature for the same material than a pilot ignition. In the first stage of the ignition process, as above described, there was no piloted source. The AW heated the target that produced flammable pyrolysis gases and ignition occurred when the gas mixture temperature reached the self-ignition temperature (step (1) as above described). Then, the accumulated flammable gases ignited (step (2)) and the fire spread over the rest of the target (step (3)).
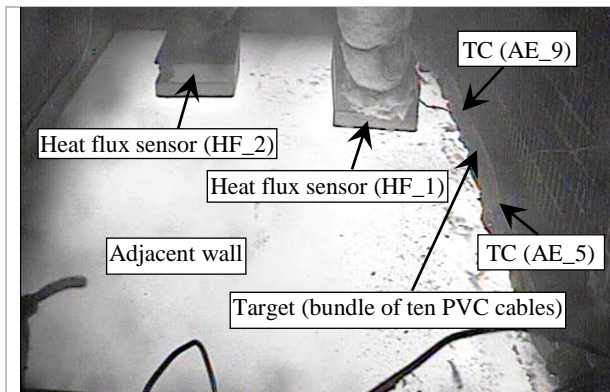

Fig. 21: Before ignition ($t = t_{ig} - 0.02\ s$) in the AE (eg, for the T2 test). AE, adjacent enclosure; HF, heat flux; PVC, poly(vinyle chloride); TC, thermocouple.
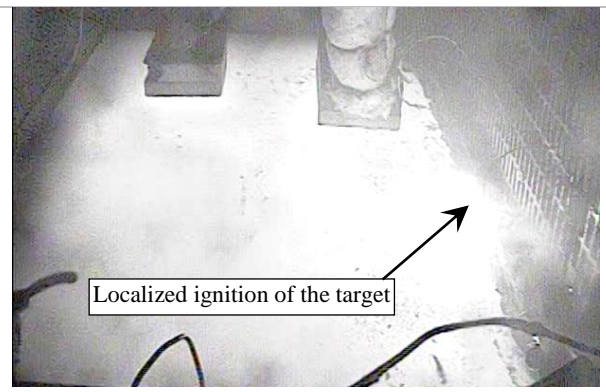
Fig. 22: Ignition of the target ($t = t_{ig}$) contained in the AE (eg, for the T2 test), AE, adjacent enclosure.

Fig. 23: Ignition of the flammable gases ($t = t_{ig} + 0.02\ s$) accumulated within all the AE (eg, for the T2 test). AE, adjacent enclosure.

Fig. 24: Fire spread overall the target ($t = t_{ig} + 0.1\ s$) contained in the AE (eg, for the T2 test). AE, adjacent enclosure.
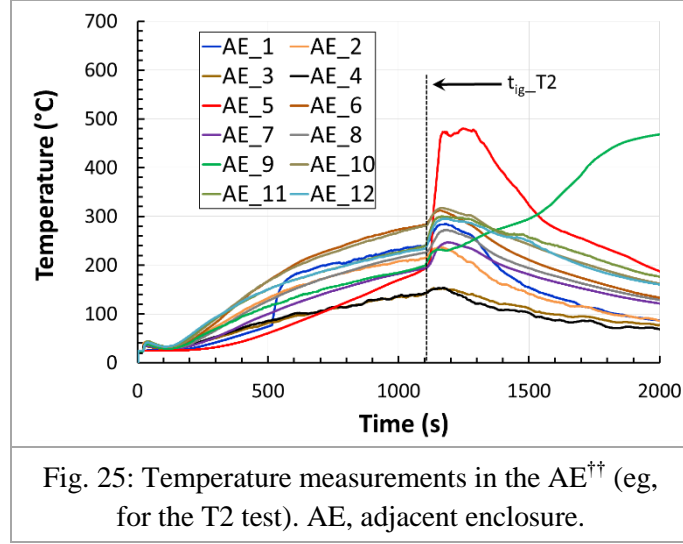
Fig. 25: Temperature measurements in the AE[††] (eg, for the T2 test). AE, adjacent enclosure.

The most commonly used ignition criterion is that related to the critical temperature[13-15]. These studies indeed mentioned that when the fuel reaches a critical surface temperature or critical ignition temperature, $T_{c,ig}$, then it can ignite. Table 6 reports for the T1 to T11 tests t_{ig}, $\dot{q}_{ig}^{"}$, $T_{av,AW}^{ig}$ and $T_{av,FW}^{ig}$. The three last parameters are $\dot{q}^{"}$, $T_{av,AW}$ and $T_{av,FW}$ measured at t_{ig}, respectively. Given that the ignition can occur anywhere along the target which was either very nearly or in contact with the AW, $T_{av,AW}^{ig}$ is assumed to estimate correctly the target temperature leading to its ignition. Furthermore, $\dot{q}_{ig}^{"}$, measured nearby the target (Fig. 7), is supposed close to the critical incident heat flux, $\dot{q}_{c,ig}^{"}$, leading to the ignition of the targets. For each target-type, best estimations of $T_{c,ig}$ and $\dot{q}_{c,ig}^{"}$ are thus calculated as the average of respective $T_{av,AW}^{ig}$ and $\dot{q}_{ig}^{"}$ measured for the related tests (Table 6):

$$T_{c,ig} = \frac{\sum_{k=1}^{j} T_{av,AW}^{ig,k}}{j} \tag{4}$$

$$\dot{q}_{c,ig}^{"} = \frac{\sum_{k=1}^{j} \dot{q}_{ig,k}^{"}}{j} \tag{5}$$

Where j is the number of the considered tests for a given target-type (j = 4, 2 and 4 for the target-type with PVC cables[‡‡], HFFR cables and TB, respectively), $T_{av,AW}^{ig,k}$ and $\dot{q}_{ig,k}^{"}$ are $T_{av,AW}^{ig}$ and $\dot{q}_{ig}^{"}$, respectively, for the test k. Moreover, $\tilde{U}(T_{c,ig})$ and $\tilde{U}(\dot{q}_{c,ig}^{"})$ can be evaluated from Eq. (4) and (5), respectively, as follows[10]:

$$\tilde{U}(T_{c,ig}) = \frac{\sqrt{\sum_{k=1}^{j} \tilde{U}(T_{av,AW}^{ig,k})^2}}{j} \tag{6}$$

[††]The AE_1, 5 and 9 temperature measurements were positioned in the target while the other ones were located outside the target, in the AE.

[‡‡] For this target-type, only the T1 to T4 tests were taken into account for the evaluation of $T_{c,ig}$ and $\dot{q}_{c,ig}^{"}$. Indeed, the last test with this target-type (ie, the T5 test) involved a mechanically ventilated AE which, as further discussed, affected $T_{av,AW}^{ig}$. In contrast, for the two other target-types, all the tests indicated in Table 6 were considered.

$$\widetilde{U}\big(\dot{q}_{c,ig}^{"}\big) = \frac{\sqrt{\sum_{k=1}^{j} \widetilde{U}(\dot{q}_{ig,k}^{"})^2}}{j} \qquad (7)$$

Where $\widetilde{U}(T_{av,AW}^{ig,k}) = 0.08$ and $\widetilde{U}(\dot{q}_{ig,k}^{"}) = 0.17$ (Table 5). Table 7 finally gives $T_{c,ig} \pm \widetilde{U}(T_{c,ig}) \cdot T_{c,ig}$ and $\dot{q}_{c,ig}^{"} \pm \widetilde{U}(\dot{q}_{c,ig}^{"}) \cdot \dot{q}_{c,ig}^{"}$ for the three target-types. $T_{c,ig}$ and $\dot{q}_{c,ig}^{"}$ are calculated from Eqs. (4) and (5), respectively, while $\widetilde{U}(T_{c,ig})$ and $\widetilde{U}(\dot{q}_{c,ig}^{"})$ are assessed from Eqs. (6) and (7), respectively. These calculations considered j = 4, 2 and 4 for the target-type with PVC cables, HFFR cables and TB, respectively, as previously explained.

Table 6 : Main test results obtained at the ignition time of the targets.

Test ID	Ignition time, t_{ig}(s)	IHF measured close to the targets at ignition, $\dot{q}_{ig}^{"}$ (kW/m²)	Average temperature of the outer walls at ignition (°C)	
			$T_{av,AW}^{ig}$ for AW	$T_{av,FW}^{ig}$ for FW
T1	739	36	530	682
T2	1109	36	520	656
T3*	1285	34	531	642
T4	1098	36	523	670
T5	1121	38	560	662
T6	1403	51	596	725
T7*	1321	43	601	699
T8	496	29	501	658
T9	811	35	517	658
T10	884	31	504	630
T11	979	29	479	636

* Repeatability test. Abbreviations: AW, Adjacent wall; FW, Fire wall; IHF, Incident heat flux.

Table 7 : Critical ignition temperature and heat flux according to the target-type.

Target	Bundle of ten PVC cables	Bundle of ten HFFR cables	Three sets of forty TB
Critical ignition temperature, $T_{c,ig}$ (°C)	526 ± 21	599 ± 34	500 ± 20
Critical ignition heat flux, $\dot{q}_{c,ig}^{"}$ (kW/m²)	35.5 ± 3	47 ± 5.5	31 ± 3

Effect of the target type

The $T_{c,ig}$ evaluation for the target-type composed with the PVC cables (526 ± 21 °C, Table 7) falls in the 500-600 °C range provided by Gong et al.[15] that studied spontaneous ignition of similar cable type (ie, PVC external sheath and XLPE insulation). Furthermore, the piloted ignition temperature was

measured at around 300°C[16] for electric cables with a PVC external sheath. Accordingly, these outcomes confirm that the target-type composed with the PVC cables spontaneously ignited.

$T_{c,ig}$ for the two other targets (599 ± 34 °C for the bundle of 10 HFFR cables and 500 ± 20 °C for the sets of TB, Table 7) are also relevant with spontaneous ignition as indicated in the studies[12-13]. These studies indeed report that for a broad variety of natural and synthetic organics solids, $T_{c,ig}$ falls in the 500-600 °C and 300-450 °C ranges for spontaneous and piloted ignitions, respectively. Moreover, piloted ignition temperature for materials made in polyamide was measured in fire calorimetry apparatus at around 300°C[17]. Furthermore, for similar HFFR electric cable-types as studied in this work (ie, cable-type containing EVA and PE as polymeric materials and ATH as HFFR), the piloted ignition temperature was estimated at about 400 °C[18].

Finally, Table 7 also shows that the values of both $T_{c,ig}$ and $\dot{q}''_{c,ig}$ measured for the targets composed with either TB or the PVC cables are similar while these ignition criteria obtained for the target made with the HFFR cables are clearly higher. These results imply that electrical components such as PVC cables or TB contained in a cabinet adjacent to a fire cabinet could ignite earlier than HFFR cables.

Effect of the air gap

Fig. 26 to Fig. 28 show, for the T1, T2, T8, T9 and T11 tests, the air gap effect on time evolutions of $T_{av,FW}$, $T_{av,AW}$ and $\dot{q}''$, respectively. t_{ig} is also indicated in those figures. The T1 and T2 tests used the target-type composed with the PVC cables while the T9, T10 and T11 tests involved that made with TB. These figures first exhibit that the air gap increase slows down the raise of both $T_{av,FW}$ and $T_{av,AW}$ (Fig. 26 and Fig. 27, respectively). Accordingly, both $T_{c,ig}$ and $\dot{q}''_{c,ig}$ are reached later as the air gap increases, which delays t_{ig}. A larger air gap indeed leads to enhance the cooling effect of air flowing between the enclosures and thus delay the rise of both $T_{av,FW}$ and $T_{av,AW}$ caused by the controlled fire.
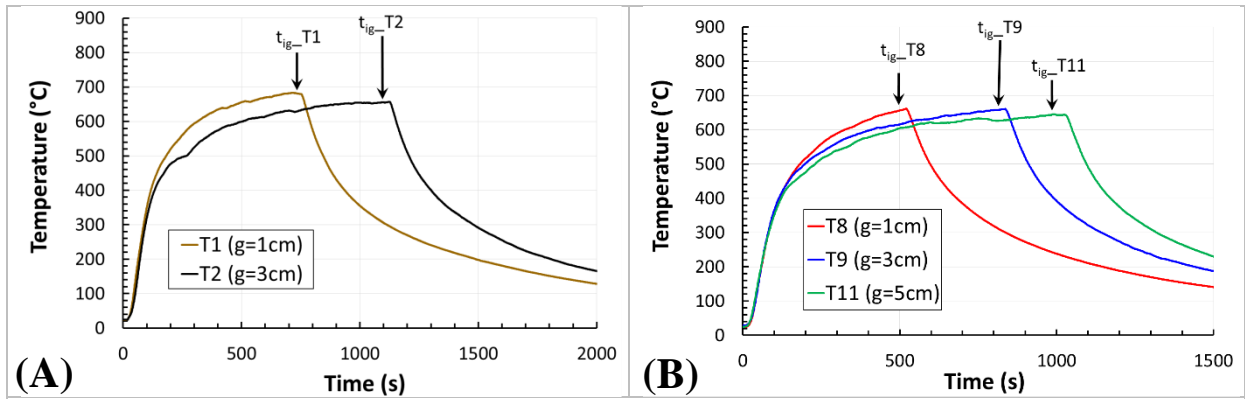

Fig. 26: Average temperature of the FW. A, T1 and T2 tests. B, T8, T9 and T11 tests. FW, fire wall.
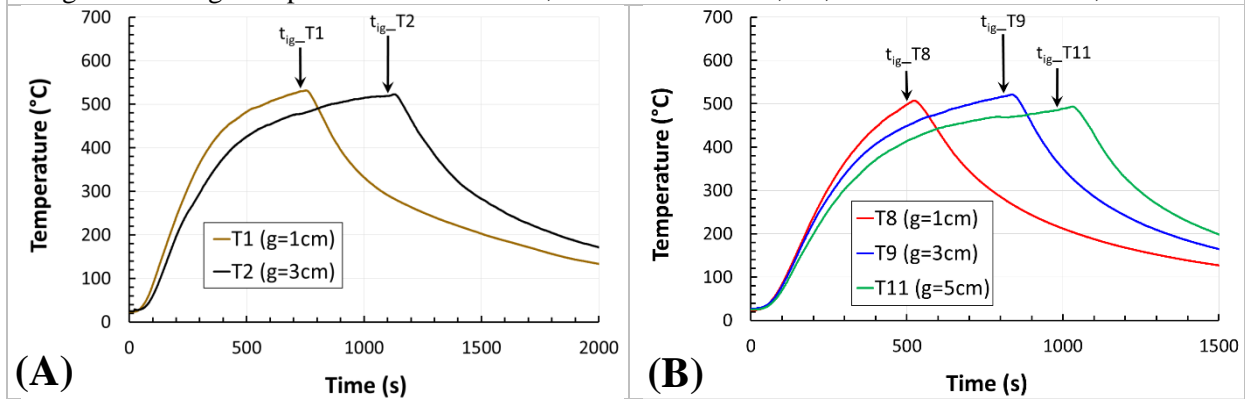

Fig. 27: Average temperature of the AW. A, T1 and T2 tests. B, T8, T9 and T11 tests. AW, adjacent wall.
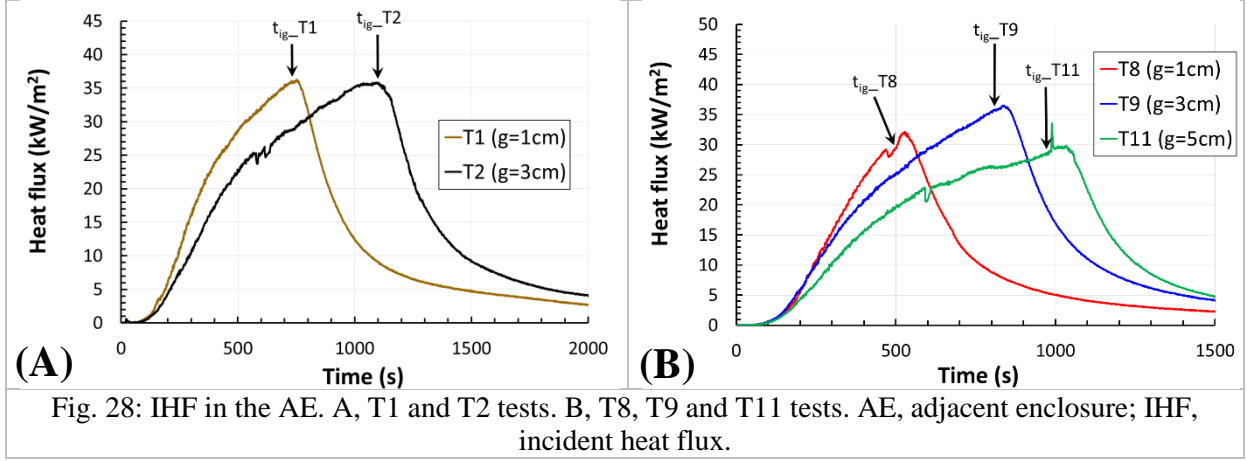
Fig. 28: IHF in the AE. A, T1 and T2 tests. B, T8, T9 and T11 tests. AE, adjacent enclosure; IHF, incident heat flux.

Effect of the ventilation mode

The effect on the ignition conditions of a natural ventilation mode in the AE, was studied using both the T2 and T4 tests. The T2 test involved a not ventilated AE (ie, the grids were fully-blocked) while for the T4 test the AE was naturally-ventilated (ie, the grids were half-blocked[§§]), as specified in Table 1 and showed in Fig. 9. Fig. 29 to Fig. 32 show for these two tests $T_{av,FW}, T_{av,AW}, \dot{q}^{"}$ and the average gas temperature in the AE ($T_{av,AE}$), respectively. $T_{av,AE}$ was assessed as the average of the twelve temperature measurements located in the AE (Table 3):

$$T_{av,AE} = \frac{\sum_{k=1}^{12} T_{AE\_k}}{12} \qquad (8)$$

The above figures exhibit that the natural ventilation as implemented in the AE has no impact on the time evolutions of $T_{av,FW}, T_{av,AW}$ and $\dot{q}^{"}$ (Fig. 29 to Fig. 31, respectively) and very small influence on time evolutions of $T_{av,AE}$ (Fig. 32). The first outcome also corroborates the good test repeatability previously highlighted with the T2/T3 and T6/T7 tests. Furthermore, t_{ig} for the T2 and T4 tests are very close. This result is relevant with the fact that both $T_{av,AW}^{ig}$ and $\dot{q}_{ig}^{"}$ for these two tests are practically identical (Table 6). Furthermore, for the T9 and T10 tests which used identical setups except the natural ventilation mode of the AE implemented for the former test (the grids were half-blocked, Table 1), $t_{ig}, \dot{q}_{ig}^{"}$ and $T_{av,AW}^{ig}$ are quite similar (Table 6). This confirms that the natural ventilation mode as used in the AE has no clear impact on the ignition conditions.

Next, the effect of a mechanical ventilation mode in the AE was investigated with the T1 and T5 tests. Indeed, the T1 test involved a not ventilated AE (ie, the grids were half-blocked) while for the T5 test the AE was mechanically-ventilated. For that purpose, a fan was connected to the lower grid (Fig. 9) that imposed a ventilation flow rate set at 165 m³/h. Fig. 33 to Fig. 36 show for these two tests time evolutions of $T_{av,FW}, T_{av,AW}, \dot{q}^{"}$ and $T_{av,AE}$, respectively. The last figure points out that the mechanical ventilation of the AE slows down the increase of $T_{av,AE}$ and therefore very likely that of the target temperature. Accordingly, the target ignition for the T5 test is delayed (Table 6). In contrast, the first three figures exhibit that time evolutions of $T_{av,FW}, T_{av,AW}$ and $\dot{q}^{"}$ are very close up to the target ignition time for the T1 test (ie, $t_{ig\_}T1$). Beyond this time, the three above parameters continue to grow, up to the ignition of the target for the T5 test, as shown in Fig. 33 to Fig. 35.

[§§]The remaining opened grid area was 0.015 m² for each ventilation grid (Fig. 9).
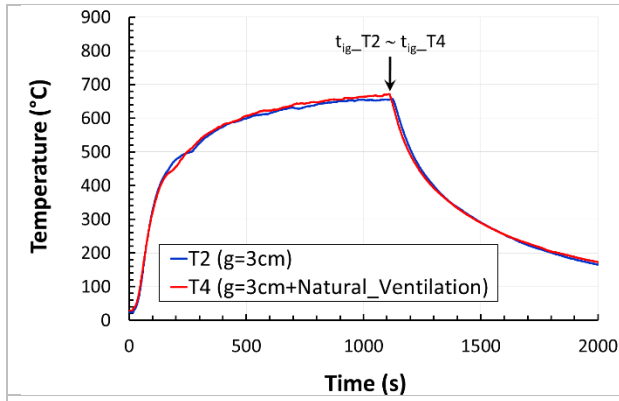
Fig. 29: Average temperature of the FW for the T2 and T4 tests. FW, fire wall.
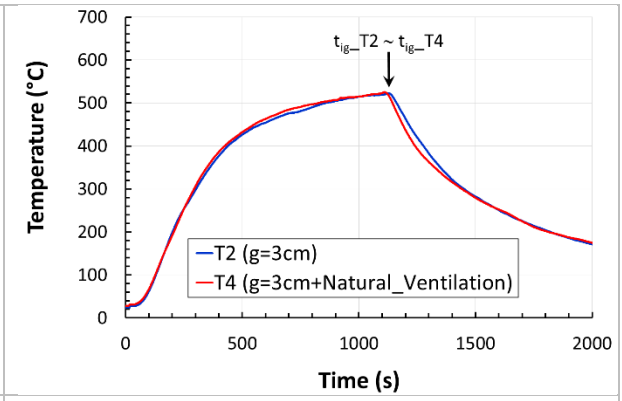

Fig. 30: Average temperature of the AW for the T2 and T4 tests. AW, adjacent wall.
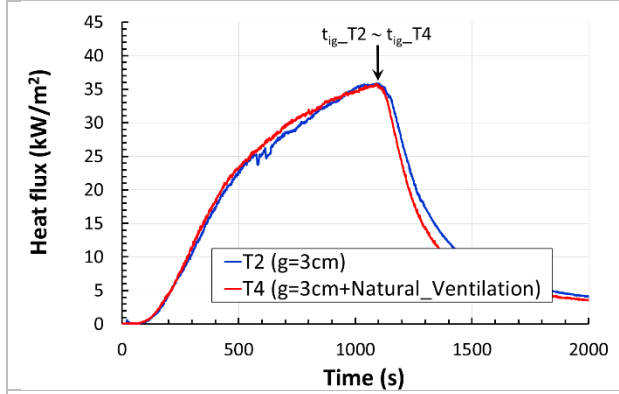

Fig. 31: IHF in the AE for the T2 and T4 tests. IHF, incident heat flux; AE, adjacent enclosure.
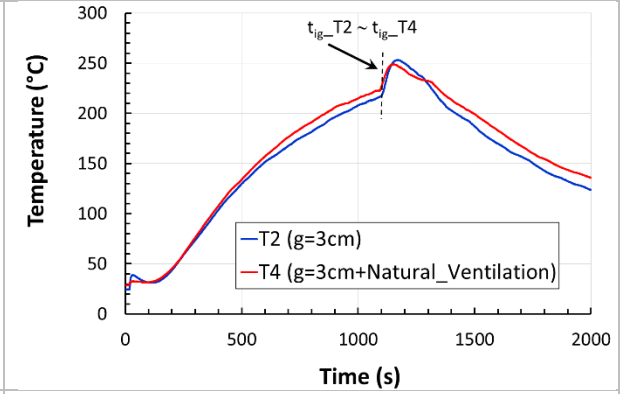

Fig. 32: Average gas temperature in the AE for the T2 and T4 tests. AE, adjacent enclosure.
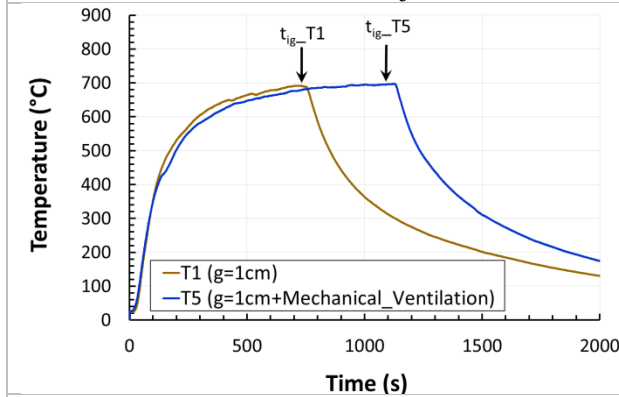

Fig. 33: Average temperature of the FW for the T1 and T5 tests. FW, fire wall.
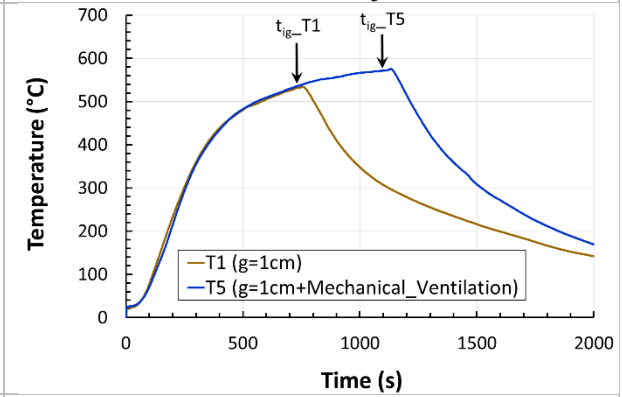

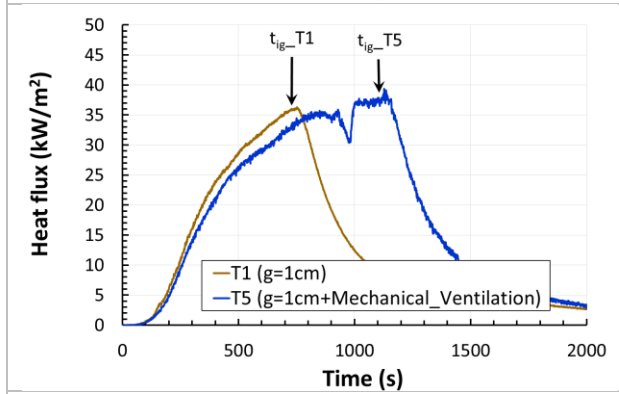Fig. 34: Average temperature of the AW for the T1 and T5 tests. AW, adjacent wall.

Fig. 35: IHF in the AE for the T1 and T5 tests. IHF, incident heat flux; AE, adjacent enclosure.
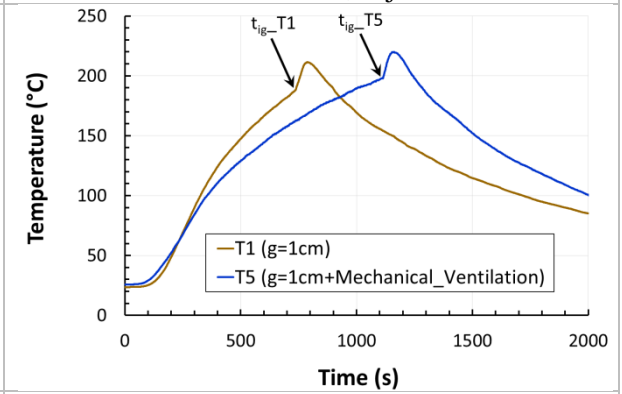

Fig. 36: Average gas temperature in the AE for the T1 and T5 tests. AE, adjacent enclosure.

The impact of the mechanical ventilation mode is due to the significant but nevertheless realistic[***] volume flow rate (165 m^3/h) as used in the AE. In contrast, for the natural ventilation mode as implemented in the AE (the grids were half-blocked and no fan was used) the volume flow rate should be clearly lower.

CONCLUSION

This study was carried out for providing new insights on the ignition of electrical components that can occur in an electrical cabinet adjacent to a burning cabinet. This work aims at investigating the impact on the ignition conditions of the air gap between two electrical cabinets (in the 1-5 cm range), the electrical component-type (bundle of electric cables or sets of terminal blocks) contained in the adjacent cabinet and its ventilation mode. For that purpose, a test device of two adjacent steel enclosures was designed using a fire field model, in order to reproduce at reduced-scale adjacent electrical cabinets used in large-scale fire tests. Eleven fire tests using this test device were carried out. First, the test repeatability was shown satisfactory and the evaluation of the measurement uncertainties was fully detailed. This study next reveals that each electrical component-type (considered as target) spontaneously ignited in the adjacent enclosure when their temperature and the incident heat flux reach critical ignition values. These ignition criteria are assessed similar for the two target-types composed with either the terminal blocks (TB) or the poly(vinyl chloride) [PVC] cables and clearly lower than those estimated for the target-type made with the halogen-free flame retardant (HFFR) cables. These results imply that electrical components such as PVC cables or TB contained in a cabinet adjacent to a fire cabinet could ignite earlier than HFFR cables. The tests also show that the air gap increase slows down the rise of the side wall temperature of the two enclosures, due to the cooling effect of air flowing between the enclosures. Accordingly, the time to ignition of the targets is delayed. This work finally highlights that the mechanical ventilation of the adjacent enclosure cools down the internal gas volume and thus the targets. This extends the required time to reach the ignition conditions of the targets. In contrast, the natural ventilation as implemented in the adjacent enclosure has small impact on these conditions. The impact of the mechanical ventilation mode is due to the significant but nevertheless realistic volume flow rate as used in the AE. In contrast, for the natural ventilation mode as implemented in the AE the volume flow rate should be clearly lower.

REFERENCES

[1]Organisation for Economic Co-operation and Development (OECD), Nuclear Energy Agency (NEA), July 2011, "OECD FIRE Database" (OECD FIRE DB 2010:1)

[2]Werner, W., Hyslop, J. S., Melly, N., Bertrand, R., Röwekamp, M., Huerta, A., 2011, Enhancements in the OECD fire database – Fire frequencies and severity of events, 21th International Conference on SMIRT, 12th International Post Conference Seminar on "Fire Safety in Nuclear Power Plants and Installations", Munich, Germany

[3]Mangs, J., Paananen, J., Keski-Rahkonen O., 2003, Calorimetric fire experiments on electronic cabinets, Fire Safety Journal, 38, p165-186

[4]Zavaleta P, Suard S, Audouin L. Fire spread from an open-doors electrical cabinet to neighboring targets in a confined and mechanically ventilated facility. Fire and Materials. 2018;1–20. https://doi.org/10.1002/fam.2685

[5]Coutin, M., 2007, Phenomenological description of actual electrical cabinet fires in a free atmosphere, 11th International Fire Science and Engineering Conference, INTERFLAM, London, UK, p725-730

[***]This value was specified according to realistic ventilation flow rates used in electrical cabinet as earlier commented.

[6]Coutin, M., Plumecocq, W., Zavaleta, P., Audouin, L., 2015, Characterization of open-doors electrical cabinet fires in compartments, Nuclear Engineering and Design, 286, p104-115

[7]Salley, M., H., Linderman, A., Refining And Characterizing Heat Release Rates From Electrical Enclosures During Fire (RACHELLE-FIRE), Volume 1: Peak Heat Release Rates and Effect of Obstructed Plume, NUREG-2178, Vol. 1, EPRI 3002005578, Avril 2016, Final Report

[8]McGrattan, K., Bareham, S., Stroup, D., Heat Release Rates of Electrical Enclosure Fires (HELEN-FIRE), NUREG/CR-7197, USNRC, Avril 2016, Final Report

[9]CALIF3S/ISIS software, Collaborative website: https://gforge.irsn.fr/gf/project/isis/

[10]JCGM 100:2008(F) GUM 1995, Evaluation of measurement data – Guide to the expression of uncertainty in measurement, September 2008

[11]A. Hamins and K. McGrattan, Verification and Validation of Selected Fire Models for Nuclear Power Plant Applications, Volume 2: Experimental Uncertainty, NUREG-1824, EPRI 1011999, Final Report, May 2007

[12]Babrauskas, V., Ignition Handbook, Fire Science Publishers/Society of Fire Protection Engineers, Issaquah WA (2003)

[13]Kanury, A.M., Flaming Ignition of Solid Fuels, ISBN:087765-451-4, Third edition, Section two, Chapter 11

[14]Vermesi, I., Roenner, N., Pironi, P., Hadden, R. M., Rein, Guillermo, Pyrolysis and ignition of a polymer by transient irradiation, Combustion and Flame 163 (2016) 31-41, http://dx.doi.org/10.1016/j.combustflame.2015.08.006

[15]Gong, T., Qiyuan, X., Huang, X., Fire behaviors of flame-retardant cables part I: Decomposition, swelling and spontaneous ignition, Fire Safety Journal 95 (2018) 113-121, http://doi.org/10.1016/j.firesaf.2017.10.005

[16]Decimus, A., Sonnier, R., Zavaleta, P., Suard, S., Ferry, L., Study of gases released under incomplete combustion using PCFC–FTIR, Journal of Thermal Analysis and Calorimetry https://doi.org/10.1007/s10973-019-08160-5

[17]Santamaria, S., Hadden, R., M., Experimental analysis of the pyrolysis of solids exposed to transient irradiation. Applications to ignition criteria, Proceeding of the Combustion Institute 37 (2019) 4221-4229, http://doi.org/10.1016/j.proci.2018.05.104

[18]Meinier, R., Sonnier, R., Zavaleta, P., Suard, S., Ferry, L., Fire behavior of halogen-free flame retardant electrical cables with the cone calorimeter, Journal of Hazardous Materials http://dx.doi.org/10.1016/j.jhazmat.2017.08.027